Journal of Membrane Science 622 (2021) 119025

Contents lists available at ScienceDirect

Journal of Membrane Science

journal homepage: http://www.elsevier.com/locate/memsci

Characterization of dextran transport and molecular weight cutoff (MWCO) of large pore size hollow fiber ultrafiltration membranes

Christopher J. Yehl, Andrew L. Zydney *

Department of Chemical Engineering, The Pennsylvania State University, University Park, PA, 16802, USA

ARTICLE INFO

Keywords:
Hollow fiber
Dextran retention
Ultrafiltration
Molecular weight cutoff
Vaccines
Virus-like particles

ABSTRACT

The development of vaccines, gene therapy agents, and virus-like particles has created exciting opportunities for the use of large pore size ultrafiltration membranes in downstream processing. One of the challenges facing both membrane producers and end-users is the difficulty in evaluating the membrane pore size or nominal molecular weight cutoff (MWCO) for the selection of appropriate membranes for targeted separations. We have used a combination of experimental measurements and theoretical modeling to develop an improved methodology for evaluating the MWCO of these large pore size ultrafiltration membranes based on dextran retention measurements. The model accounts for both concentration polarization effects and the intrinsic dextran retention behavior. The results not only provide fundamental insights into the factors controlling dextran retention, but they can also guide membrane manufacturers and end-users to the most appropriate conditions (i.e. feed flow rate and permeate flux) for evaluating the MWCO for hollow fibers with different geometry, pore size, and permeability.

1. Introduction

There is growing interest in the application of large pore size ultrafiltration membranes for the purification of novel biotherapeutics including conjugated vaccines [1–5], virus-like particles [6–8], and various nucleic acid-based biopharmaceuticals [3,9]. Large pore size hollow fiber membrane modules are of particular interest in many of these applications due to their high packing density (large membrane area per unit volume), relatively low cost, and the lower degree of fouling due to the open channel design. Hollow fiber modules have been successfully used for the recovery and concentration of HIV vaccines produced in insect cells [10], the purification of supercoiled plasmid DNA [11], and the removal of excess polysaccharide in the production of a pneumococcal conjugate vaccine [12].

The most common method for evaluation of the pore size distribution and retention characteristics of ultrafiltration membranes is the dextran retention test [13,14] in which the membrane is challenged with a mixture of dextrans spanning the size range appropriate for the particular membrane. Several studies have demonstrated that the pore size evaluated using dextran retention measurements are in good agreement with independent estimates determined by liquid-liquid porosimetry [15] and field emission scanning electron microscopy [16].

There are a number of challenges in the application of dextran retention tests for larger molecular weight cutoff (MWCO) membranes. This includes the high degree of concentration polarization for the large dextrans (due to the small value of the mass transfer coefficient) as well as the difficulties in using size exclusion chromatography for analysis of the molecular size distribution of these large solutes. In addition, hollow fiber modules can have large variations in filtrate flux with axial position due to the large pressure drop arising from flow through the module. This can cause back-filtration (or Starling flow) to occur during operation at the low filtrate flux typically used to minimize concentration polarization effects during the dextran challenge [17]. Bakhshayeshi et al. [18] proposed a strategy for the characterization of large MWCO hollow fiber ultrafiltration membranes that balanced the effects of backfiltration and concentration polarization while also minimizing the required filtration time for each test. This “optimized” dextran test employed very low feed and permeate flow rates, conditions that are far removed from the operating modality relevant to most end users. This creates significant challenges in the interpretation of the resulting dextran curves, significantly reducing the usefulness of the dextran test.

The objective of this study was to develop more effective protocols for evaluating the dextran retention curves of large molecular weight

* Corresponding author. 404 Chemical and Biomedical Engineering Building, Department of Chemical Engineering, The Pennsylvania State University, University Park, PA, 16802, USA.
E-mail address: zydney@engr.psu.edu (A.L. Zydney).

https://doi.org/10.1016/j.memsci.2020.119025
Received 3 November 2020; Received in revised form 21 December 2020; Accepted 23 December 2020
Available online 31 December 2020

Notation

a	Dextran radius (m)
A	Membrane area (m^2)
C_b	Concentration of solutes in the bulk/feed (g L^{-1})
C_f	Concentration of solutes in the filtrate/permeate (g L^{-1})
C_w	Concentration of solutes at the membrane wall (g L^{-1})
D	Dextran diffusion coefficient (m^2 s^{-1})
J_v	Filtrate flux (L m^{-2} h^{-1})
k_B	Boltzmann's Constant (m^2 kg s^{-2} K^{-1})
k_m	Mass transfer coefficient (m s^{-1})
L	Effective length of hollow fiber (m)
L_p	Membrane hydraulic permeability (m)
MW	Molecular weight (kDa)
$MWCO$	Molecular weight cutoff (kDa)
N	Number of fibers
Q_{feed}	Feed flow rate (mL min^{-1})
Q_p	Permeate flow rate (mL min^{-1})
R	Inner radius of hollow fibers (m)
s	Ratio of pore volume to surface area (m)
S_a	Actual membrane/dextran sieving coefficient
S_o	Observed membrane sieving coefficient
T	Temperature (K)
Greek Symbols	
$\dot{\gamma}$	Wall shear rate (s^{-1})
ΔP	Transmembrane Pressure drop (Pa)
μ	Solution viscosity (Pa s)

cut-off hollow fiber membranes using a combination of experimental measurements and theoretical modeling. The results provide fundamental insights into the factors controlling dextran retention and the calculated MWCO, while at the same time providing guidance to membrane manufacturers and end-users on the most appropriate conditions (i.e. feed and permeate flux) for evaluating the MWCO for hollow fibers with different geometry, pore size, and permeability.

2. Materials and methods

Membranes were challenged with a "cocktail" containing a mixture of several different MW dextrans: 0.2 g/L of Dextran T10 (9–11 kDa), 0.2 g/L of Dextran T40 (35–45 kDa), 0.8 g/L of Dextran T150 (150 kDa), and 1.8 g/L of Dextran T2000 (2000 kDa), obtained from Sigma-Aldrich (St. Louis, MO) and TCI Chemical (Portland, OR). The higher concentrations of the larger MW dextrans were used to obtain accurate data for the permeate concentrations of these more highly retained species, which also have a broader polydispersity than the lower MW dextrans. The dextrans were dissolved in a 1x PBS buffer at pH ≈ 7.4, which was prepared by dilution of 10x phosphate buffer stock solution (Thermo Scientific, Waltham, MA) with deionized (DI) water from a Millipore Direct-Q water purification system (Burlington, MA). All solutions were pre-filtered through 0.2 μm polyvinylidene fluoride (PVDF) membranes prior to use to remove any particulates.

Experiments were performed using Xampler (Cytiva Life Sciences, Marlborough, MA) hollow fiber modules with surface area of 110 cm^2 and MWCO of approximately 750 kDa (as provided by the manufacturer). The modules were mounted in a horizontal orientation with the feed solution introduced into the lumen-side inlet (Fig. 1). Data were obtained in total recycle mode, with both the retentate and permeate exit lines recycled back to the stirred feed reservoir to maintain a constant feed concentration throughout the experiment. Feed and permeate flow rates were controlled using two Masterflex L/S peristaltic pumps (Cole-Parmer, Vernon Hill, IL.) fitted with platinum-cured silicone tubing (Cole-Parmer). The pumps were calibrated before each experiment by timed collection using a digital balance. Pressures were monitored throughout the experiments using digital pressure gauges (Ashcroft, Stratford, CT) located immediately before and after the inlet/outlet ports.

The modules were first flushed with DI water. The membrane hydraulic permeability:

$$L_p = \frac{Q_p \mu}{A \Delta P} \tag{1}$$

was then evaluated using data for the permeate flow rate (Q_p) at several transmembrane pressure drops (ΔP), where μ is the solution viscosity and A is the membrane area. The module was then flushed with 1x PBS buffer before challenging with the dextran cocktail. Data were obtained over a range of feed and permeate flow rates (as discussed subsequently), with samples taken from the feed reservoir and permeate/retentate lines after the system had stabilized.

Dextran concentrations were evaluated using an Agilent 1260 infinity II HPLC system (Agilent Scientific instruments, Santa Clara, CA) based on refractive index (RI) measurements. In order to accurately separate dextrans over the full range of MW, the system used Ultrahydrogel 2000, 500 and 120 columns in series (Waters Corp, Milford, MA), with a guard column placed immediately before the Ultrahydrogel 2000. The HPLC was operated at a constant flow rate of 0.6 mL/min,

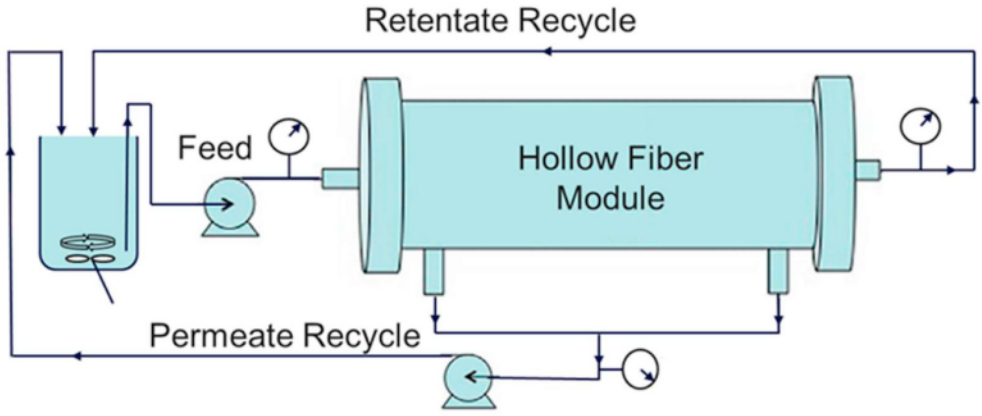

Fig. 1. Schematic of experimental setup used for dextran retention tests. Feed, retentate, and permeate pressure gauges were at same height to eliminate contributions from the gravitational head.

with the column temperature maintained at 30 °C. Samples were injected every 60–90 min. Calibration curves were constructed using EasiVial polyethylene oxide (PEO) calibration standards (Agilent Scientific instruments). The PEO standards provided much sharper peaks with lower polydispersity than the corresponding dextran standards (this is discussed in further detail in the Appendix). A calibration curve was constructed by plotting the logarithm of the PEO MW as a function of retention time yielding a highly linear relation with $R^2 > 0.99$.

3. Results and analysis

Typical experimental data from a dextran challenge experiment performed at a constant feed flow rate of 300 mL/min and a permeate flow rate of 4 mL/min, corresponding to a filtrate flux of 6.1 μm/s or 22 L/m^2/h (LMH) are shown in Fig. 2. The mean transmembrane pressure under these conditions was only 10 kPa, reflecting the high permeability of these large MWCO membranes ($L_p = 1.7 \times 10^{-12}$ m). The dextran profiles span from 28 to 47 min, corresponding to molecular weights of 1.4–2000 kDa based on the calibration curve constructed with the PEO standards. The feed and retentate profiles were nearly identical due to the very low conversion (ratio of permeate to feed flow rates). The dextran concentrations in the retentate were slightly larger than those in the feed due to dextran retention by the membrane. The permeate concentrations are well below those in the feed for the larger MW dextrans (shorter elution times), with the feed, retentate, and permeate profiles looking very similar for t > 40 min (corresponding to dextrans with MW < 21 kDa).

The chromatogram in Fig. 2 was used to evaluate the observed dextran sieving coefficients (S_o) as follows. First, the RI signal was converted to a dextran concentration by evaluating the area under the curve for the permeate, feed, and retentate samples, in each case using a thin "slice" of the chromatogram at a given elution time. Then, the elution time was converted into an effective dextran MW using a calibration curve constructed with the PEO standards as shown in the Appendix. The observed sieving coefficients were evaluated from the ratio of the dextran concentration in the permeate to that in the bulk solution, with the latter evaluated from the average of the dextran concentrations in the feed and retentate, i.e., $S_o = C_f/C_b$. Results are shown in Fig. 3 for several values of the effective wall shear rate:

$$\dot{\gamma} = \frac{4Q_{feed}}{N\,\pi\,R^3} \tag{2}$$

where N = 13 and R = 0.0005 m are the number and inner radius of the hollow fibers, respectively. Equation (2) assumes laminar flow of a Newtonian fluid consistent with literature data for the rheological properties of dextran solutions with similar MW, concentrations, and shear rates [19]. However, this equation neglects the change in feed flow rate due to the filtration as well as any variations in viscosity associated with concentration polarization. In each case, the permeate flow rate was chosen to be slightly above the minimum value required to avoid back-filtration [18]:

$$\frac{Q_p}{Q_{feed}} \geq \frac{8L_pL^2\mu}{R^3} \tag{3}$$

where L = 0.3 m is the length of the hollow fiber. The dextran sieving profiles shift up and to the right with increasing shear rate (corresponding to increasing values of the permeate flow rate to satisfy Equation (3)). In addition, the curves become much steeper as they approach the x-axis. This is discussed in more detail subsequently. The curves are each labeled with the calculated nominal "MWCO" of the module, defined as the value of the dextran MW at which $S_o = 0.1$. The use of 90% rejection to define the MWCO is fairly standard across the industry. The calculated MWCO is highly dependent on the operating conditions, with values ranging from <200 kDa to more than 1200 kDa for the conditions examined in Fig. 3.

A corresponding series of experiments at different permeate flow rates, keeping the feed flow rate fixed at 600 mL/min (corresponding to a shear rate of 8000 s^{-1}), are shown in Fig. 4. The transmembrane pressure (TMP) drop across the membrane during these experiments ranged from 14 to 90 kPa. The relatively low values of the TMP reflect the high permeability of the membrane. The observed dextran sieving profiles shift up and to the right with increasing permeate flow rate, with the curves again becoming steeper at the larger values of Q_p. The calculated MWCO for the different conditions ranges from 190 kDa at

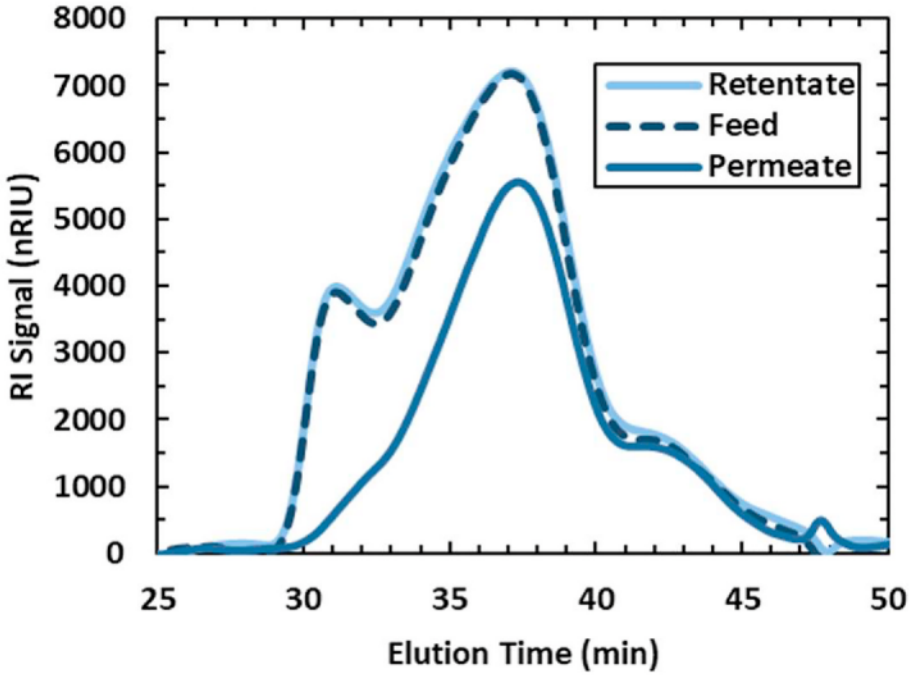

Fig. 2. HPLC profiles for dextran samples from the feed, retentate, and permeate for a dextran challenge performed at Q_{feed} = 300 mL/min and Q_p = 4 ml/min (J_v = 22 LMH) using the Xampler module.

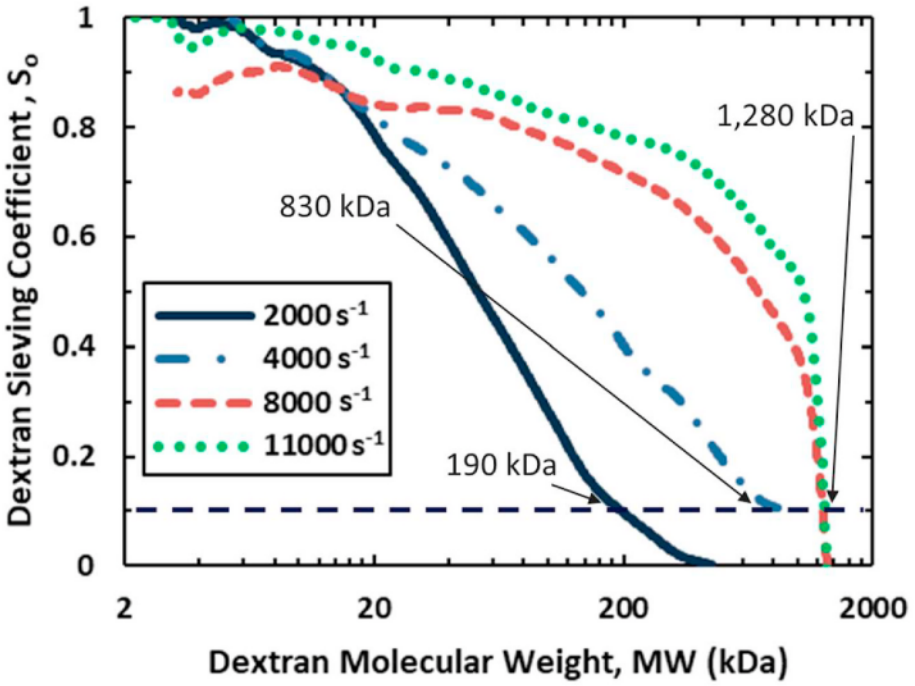

Fig. 3. Observed dextran sieving coefficient as a function of the dextran MW for the Xampler module at several values of the effective wall shear rate. The labels show the MWCO determined as the dextran MW at which $S_o = 0.1$. Permeate flow rates were increased from 1.7 mL/min to 4, 10, and 13 mL/min with increasing shear rates.

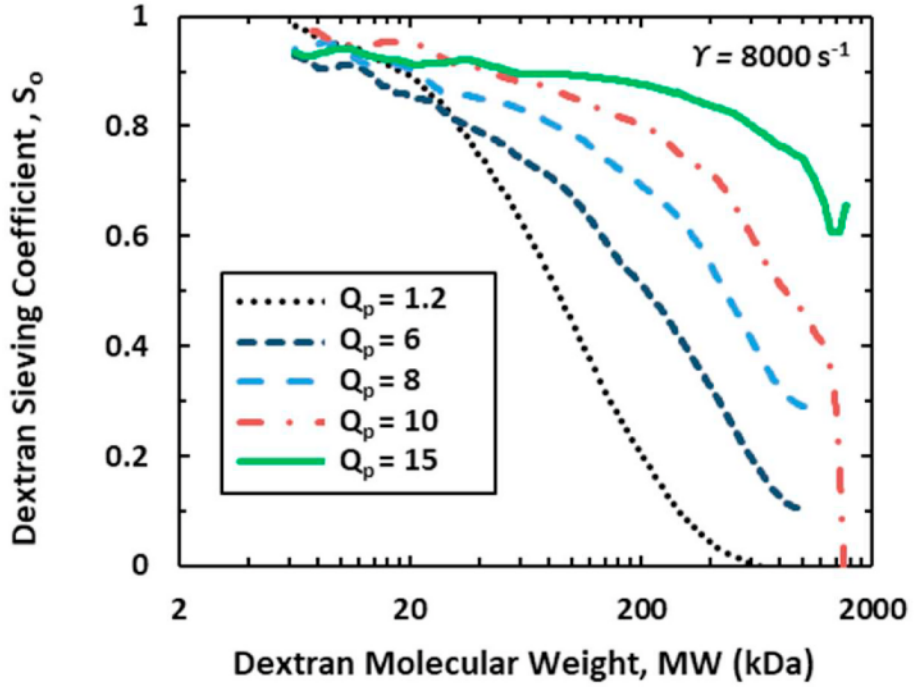

Fig. 4. Observed dextran sieving profiles for the Xampler module at an effective wall shear rate of 8000 s^{-1} at different permeate flow rates (in mL/min).

$Q_p = 1.7$ mL/min ($J_v = 9.3$ LMH) to 1280 kDa at $Q_p = 10$ mL/min ($J_v = 55$ LMH). Note that it was not possible to determine the MWCO at the highest permeate flow rate because the dextran sieving coefficient began to increase at MW > 1280 kDa. The increase in the dextran sieving coefficient with increasing permeate flow rate is due to concentration polarization effects [18]. In this case, the dextran concentration at the upstream surface of the membrane increases with increasing Q_p, leading to an increase in the permeate concentration and in turn S_o. Note that the value of $Q_p \approx 1.2$ mL/min is consistent with the permeate flow rate recommended by Bakhshayeshi et al. [18] in their optimized dextran retention test based on minimizing the extent of concentration polarization.

3.1. Model development

The results in Figs. 3 and 4 clearly demonstrate that the calculated

value of the membrane MWCO is highly dependent on the operating conditions used to evaluate the dextran retention profile. The key question is how to best perform the dextran retention test to obtain consistent and meaningful characterization of the membrane. In order to explore this more quantitatively, a mathematical framework was developed to describe the dextran sieving behavior in the hollow fiber module. The extent of concentration polarization was evaluated using the classical stagnant film model [20] with the observed dextran sieving coefficient (S_o) evaluated in terms of the filtrate flux (J_v) as:

$$S_o = \frac{S_a}{(1 - S_a)exp\left(-J_v/k_m\right) + S_a} \tag{4}$$

where S_a is the actual dextran sieving coefficient, equal to the ratio of the dextran concentration in the permeate to that in the solution immediately upstream of the membrane, and k_m is the mass transfer coefficient [20]:

$$k_m = 0.816\left(\frac{D^2\dot{\gamma}}{L}\right)^{1/3} \tag{5}$$

where $\dot{\gamma}$ is the shear rate, D is the dextran diffusion coefficient, and L is the membrane length. The actual sieving coefficient for the different MW dextrans is a function of both the dextran size and the membrane pore size distribution. Mochizuki and Zydney [14] developed a simple model for the actual sieving coefficient based on the partitioning of a spherical solute into a porous media formed by the intersection of a random array of parallel planes [21]:

$$S_a = exp\left(-\frac{a}{s}\right) \tag{6}$$

where s is the ratio of the pore volume to the pore surface area, which provides a measure of the effective pore size, and a is the dextran radius, which can be evaluated using the Stokes-Einstein equation:

$$a = \frac{k_B T}{6\pi\mu D} \tag{7}$$

where k_B is Boltzmann's constant, T is the absolute temperature, and D is the dextran diffusion coefficient [22]:

$$log_{10}(D) = -8.1154 - 0.47752 log_{10} MW \tag{8}$$

where D is in m^2/s and MW is in Da. Equations (6)–(8) have been shown to provide a good qualitative model for dextran sieving through ultrafiltration membranes without need to evaluate the detailed pore size distribution of the membrane [14].

Fig. 5 shows a comparison of the calculated MWCO of the Xampler membrane determined from the data in Fig. 3 and the model calculations based on Equations (4)–(8). In this case a value of s = 3.2 nm was used (which was chosen to obtain a reasonable fit to the measured MWCO at the lowest shear rate), with the mass transfer coefficient given by Equation (5) increased by a factor of 2.5 based on previous results for dextran mass transfer in similar hollow fiber modules [17]. The model and data are in good qualitative agreement, with the MWCO varying by more than a factor of 5. The discrepancy seen at the intermediate shear rate reflects the simplifications in the model equations used to describe both the actual sieving coefficient and the extent of concentration polarization, including the details of the pore size distribution and the effects of intermolecular interactions on bulk dextran transport. The model calculations for the dextran retention profiles also capture the same trends seen in Figs. 3 and 4, providing further confirmation of the general model framework.

3.2. Dextran retention test

The results in Fig. 5 clearly demonstrate the need to identify controlled experimental conditions for evaluating the dextran retention

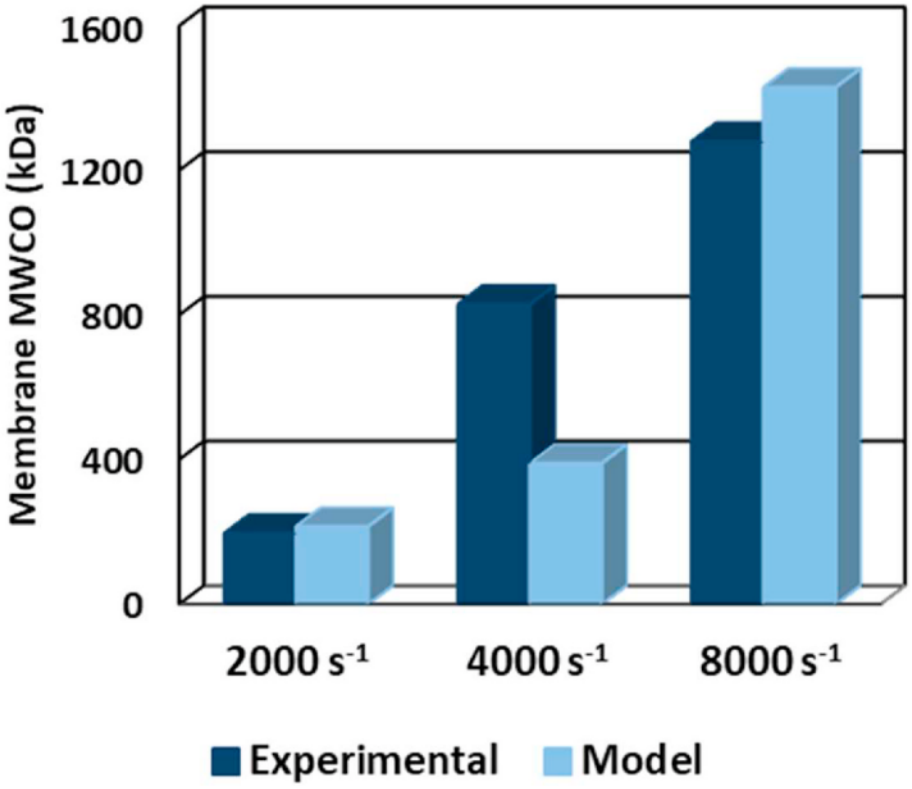

Fig. 5. Comparison of experimental data and model calculations for the observed MWCO for the Xampler module at effective wall shear rates of 2000 s^{-1} (with Q_p = 1.7 mL/min), 4000 s^{-1} (with Q_p = 4.0 mL/min), and 8000 s^{-1} (with Q_p = 10 mL/min).

profile and the membrane MWCO. The approach described by Bakhshayeshi et al. [18] was based on minimizing the extent of concentration polarization so that the observed sieving coefficient was only slightly larger than the actual sieving coefficient. However, there are three disadvantages to this approach. First, the use of very low filtrate flux means that long filtration times are required to effectively wash-out the dead volume in the shell space of the hollow fiber module. This is a particular issue in small scale modules commonly used for running quality control tests on fiber lots since the individual fibers tend to be very loosely packed in these modules (large shell volume relative to the membrane area). Second, end-users almost never operate these high permeability membranes at such low filtrate flux. Thus, the measured values of the retention coefficient are likely to be of little direct relevance to commercial applications of these hollow fiber modules. Finally, the dextran retention curve under these conditions is quite diffuse (spanning a large range of dextran molecular weight). Thus, small errors in the measured values of the dextran concentration can lead to significant discrepancies in the calculated value of the MWCO. In contrast, the dextran retention curves at high filtrate flux are very steep (Fig. 4), particularly in the region near 90% rejection, significantly increasing the accuracy of the calculated MWCO.

The argument presented above might suggest that one should use the highest possible filtrate flux to evaluate the dextran retention profile. However, the high degree of concentration polarization under these conditions can lead to membrane fouling and it can also generate odd artifacts in the dextran retention curve as shown by an increase in the dextran sieving coefficient with increasing dextran MW (as seen in the curve at the highest permeate flow rate in Fig. 4). This latter effect is also predicted by the model developed in the previous section.

The conditions leading to an increase in S_o with increasing dextran size can be estimated using the previously presented model framework as follows. For small values of the actual sieving coefficient, Equation (4) can be approximated as:

– — (9)

by taking S_a 1 in the denominator. The derivative of the sieving coefficient with respect to dextran size is thus:

— — – — — (10)

The derivative of the mass transfer coefficient with respect to dextran radius can be evaluated directly from Equation (5) with the diffusivity given by Equation (7) as:

— – — (11)

Substitution of Equation (11) into Equation (10) gives:

— — – – — (12)

At small values of the filtrate flux, the derivative is always negative, i.e., the sieving coefficient decreases with increasing dextran size as expected. However, at large degrees of polarization, Equation (12) predicts that the dextran sieving coefficient can increase with increasing dextran size (as seen in Fig. 4). This artifact in the dextran sieving curve can be avoided by performing the dextran challenge at:

— – – – (13)

where the last expression is developed using the expression for the actual sieving coefficient as a function of the dextran radius (Equation (6)). Since we are most interested in the behavior of the dextran sieving curve at a rejection coefficient near 90%, i.e., when S_a 0.1, Equation (13) corresponds to:

— (14)

Bakhshayeshi et al. [18] evaluated the effective diffusion coefficient of a 1000 kDa dextran as D 8.6 10 ^{11} m^2/s, which gives k_m 3.1 10 ^{6} m/s at a shear rate of 8000 s^{-1}. Equation (13) thus gives a filtrate flux of J_v 59 LMH or Q_p 12 mL/min. These results are in excellent agreement with the data in Fig. 4. The retention curve at Q_p 10 mL/min shows the steepest slope while the curve at Q_p 15 mL/min shows a reversal in slope at a dextran MW around 1500 kDa.

The two key constraints that must be satisfied for an effective dextran retention test are shown in Fig. 6. The solid line shows the minimum filtrate flux required to avoid back-filtration (given by the inequality in Equation (3)) while the dashed curve shows the maximum filtrate flux required to eliminate a reversal in slope of the dextran retention curve (given by the inequality in Equation (14)). The region between these curves defines the potential operating conditions for the dextran retention test. At very high shear rates (23,000 s^{-1}), it is impossible to effectively design a dextran retention test the permeate flow rate needed to avoid back-filtration causes unacceptable concentration polarization leading to a reversal in the slope of the dextran retention curve. The black symbol in Fig. 6 shows the operating conditions for the optimized dextran retention test recommended by Bakhshayeshi et al. [18]. As discussed previously, these conditions are not relevant to commercial bioprocessing and they result in a very diffuse dextran sieving curve. The shaded oval shows conditions that satisfy both operating constraints (the inequalities given by Equations (3) and (13)) while providing the steep dextran retention curves needed to obtain very accurate and robust values for the membrane MWCO.

4. Conclusions

Although dextran retention tests have been used for the characterization of ultrafiltration membranes for more than 30 years, the application of this methodology to large pore size hollow fiber membranes has been problematic due to the large axial pressure drop and the high membrane permeability. The results presented in this paper provide a rational framework for the development of a robust dextran retention test that can be used to evaluate the MWCO, develop appropriate quality control tests, and support end-users in initial screening/selection of large pore size membranes.

From an experimental perspective, we developed a calibration curve for the SEC column using PEO standards instead of dextrans, with the much narrower PEO providing more accurate and reproducible results for the dextran retention curve. Although it would have been possible to use PEO instead of dextrans for the membrane characterization, previous studies have demonstrated that PEO tends to elongate during ultrafiltration, allowing large PEO molecules to pass through very small pore size ultrafiltration membranes [23]. This makes it very difficult to extrapolate from data for PEO to describe the behavior of protein complexes, viruses, or nanoparticles that generallygeneg show minimal elongation under typical ultrafiltration conditions.

The experimental data and model calculations clearly demonstrate the importance of concentration polarization on both the shape and magnitude of the dextran retention curves, with the calculated MWCO a function of both the feed flow rate (or shear rate) and the permeate flux. A simple mathematical model was developed that accounts for these phenomena, allowing us to identify an effective window for evaluating the MWCO. This window avoids back-filtration, which sets the lower bound on the permeate flux (at a given feed flow rate) but exploits concentration polarization to obtain a steeper dextran retention curve and thus a more robust value for the membrane MWCO. The size of this window decreases as the membrane pore size (or nominal MWCO) increases: the increase in membrane permeability shifts the lower bound up while the increase in the size of the dextran with 90% rejection shifts

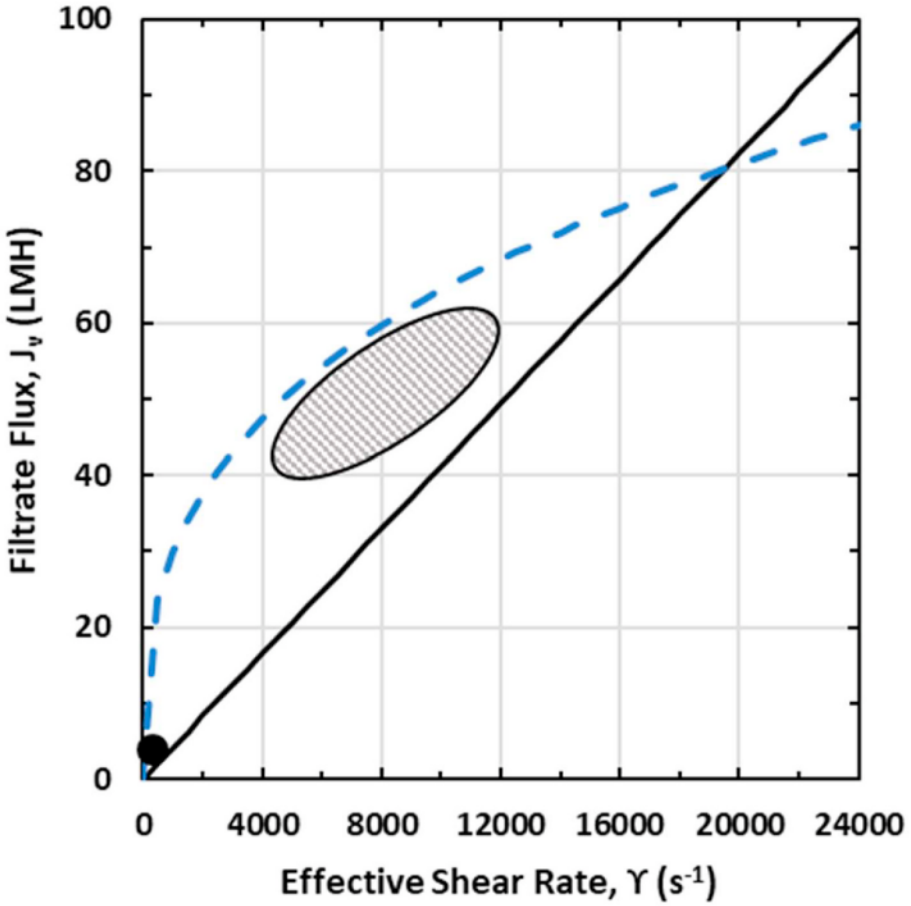

Fig. 6. Operating constraints on the dextran retention test for the Xampler module based on Eqs. (3) and (13) with N = 13, L = 0.3 m, R = 0.0005 m, and $L_p = 1.7 \times 10^{-12}$ m. Filled black symbol shows conditions recommended by Bakhshayeshi et al. [18] while the shaded oval represents the preferred operating conditions from the current work.

the upper bound down (due to the reduction in the value of the mass transfer coefficient). This operating window is also a function of the hollow fiber geometry, with the fiber radius and length affecting both the conditions needed to avoid back-filtration as well as the extent of concentration polarization. The ability to more effectively evaluate/characterize these large pore size membranes should greatly facilitate their development and application in the downstream processing of a range of important biotherapeutics including conjugate vaccines, virus-like particles, and gene therapy agents.

Author Statement

Christopher J. Yehl: Data curation, Formal analysis, Investigation, Writing – original draft. Andrew L. Zydney: Conceptualization, Funding acquisition, Supervision, Writing – review & editing.

Declaration of competing interest

The authors declare that they have no known competing financial interests or personal relationships that could have appeared to influence the work reported in this paper.

Acknowledgements

The authors would like to acknowledge financial support provided by Cytiva Life Sciences through the Membrane Science, Engineering, and Technology (MAST) Center, which is funded by grant number 1841474 from the NSF IUCRC program. Technical support from Wei Yuan and Inova Strug at Cytiva was invaluable for this project.

Appendix

Figure A1 shows a comparison of the SEC profiles for two of the EasiVial PEO standards (MW of 544 and 109 kDa) with that of a 490 kDa dextran standard obtained from American Polymer standards (Mentor, Ohio). All conditions for the SEC were identical. The peaks for the PEO standards were much sharper than that for the dextran, even for the much larger PEO standard (retention time of 31 min versus 35 min for the dextran). This difference is also seen in the reported values for the polydispersity, which ranged from 1.02 to 1.05 for the PEO standards compared to as much as 1.5 for the larger MW dextrans. The sharper peaks for the PEO led to more accurate calibration curves for evaluating the dextran retention as a function of dextran size, although the reported values for the dextran MW given in this paper are only "effective" MW since they were determined based on the PEO standards.

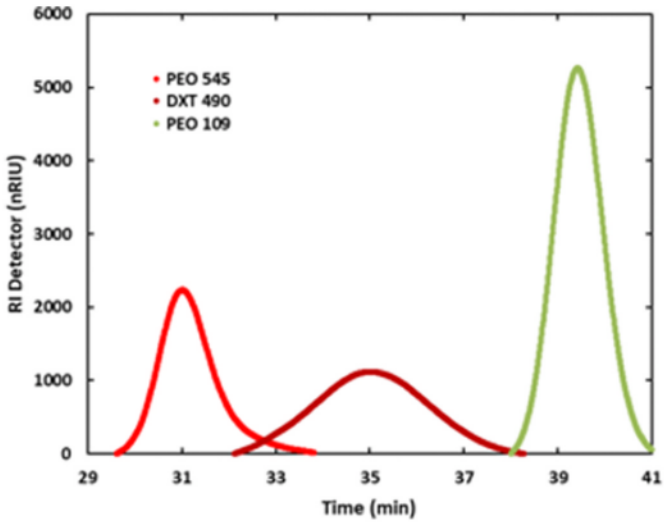

Fig. A1. SEC profiles for PEO standards (545 kDa and 109 kDa) along with that for a dextran standard (490 kDa).

A typical calibration curve for the Ultrahydrogel 2000, 500, and 150 columns in series is shown in Figure A2. In each case, the data are plotted at the manufacturer's value for the MW of the PEO using the retention time evaluated at the peak maximum. The logarithm of the PEO retention time was highly linear in the PEO molecular weight with $R^2 > 0.998$. The calibration curve constructed from the linear regression fit to the data was used to evaluate the effective MW of the different dextran "slices" for the chromatographs shown in Fig. 2.

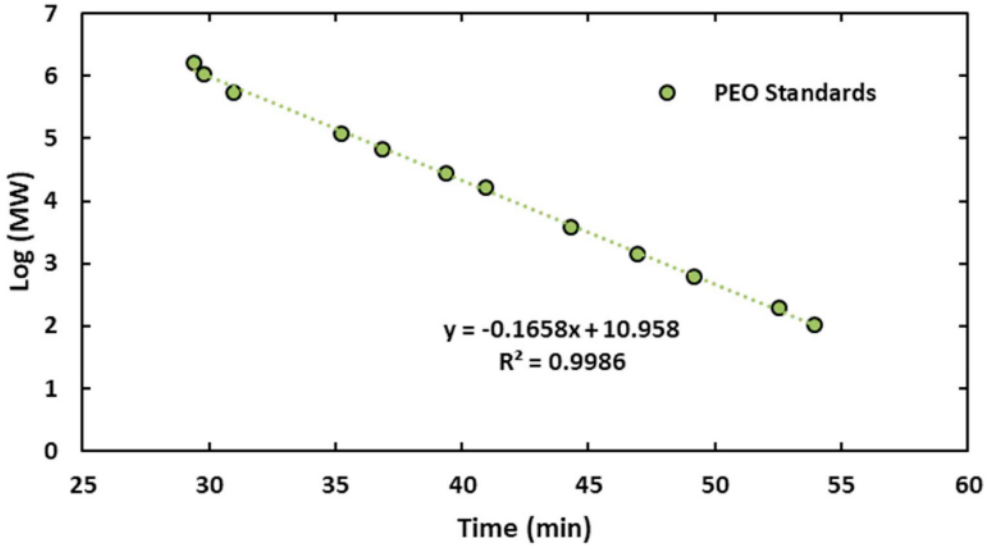

Fig. A2. Typical calibration curve for the Ultrahydrogel 2000, 500 and 150 columns in series constructed using PEO standards.

References

[1] P. Emami, S.P. Motevalian, E. Pepin, A.L. Zydney, Purification of a conjugated polysaccharide vaccine using tangential flow diafiltration, Biotechnol. Bioeng. 116 (2019) 591–597, https://doi.org/10.1002/bit.26867.

[2] M. Hadidi, J.J. Buckley, A.L. Zydney, Ultrafiltration behavior of bacterial polysaccharides used in vaccines, J. Membr. Sci. 490 (2015) 294–300, https://doi.org/10.1016/j.memsci.2015.04.047.

[3] V.M.M. Goncalves, M. Takagi, R.B. Lima, H. Massaldi, R.C. Giordano, M. M. Tanizaki, Purification of capsular polysaccharide from Streptococcus pneumoniae serotype 23F by a procedure suitable for scale-up, Biotechnol. Appl. Biochem. 37 (2003) 283, https://doi.org/10.1042/ba20020075.

[4] C. Gerke, A.M. Colucci, C. Giannelli, S. Sanzone, C.G. Vitali, L. Sollai, O. Rossi, L. B. Martin, J. Auerbach, V. Di Cioccio, A. Saul, Production of a Shigella sonnei vaccine based on generalized modules for membrane antigens (GMMA), 1790GAHB, PloS One 10 (2015), https://doi.org/10.1371/journal.pone.0134478.

[5] Z. Kis, R. Shattock, N. Shah, C. Kontoravdi, Emerging technologies for low-cost rapid vaccine manufacture 14, Biotechnol. J., 2019, 1800376.

[6] H. Nazem-Bokaee, F. Fallahianbijan, D. Chen, S.M. O'Donnell, C. Carbrello, S. Giglia, D. Bell, A.L. Zydney, Probing pore structure of virus filters using scanning electron microscopy with gold nanoparticles, J. Membr. Sci. 552 (2018) 144–152, https://doi.org/10.1016/j.memsci.2018.01.069.

[7] S.B. Carvalho, R.J.S. Silva, M.G. Moleirinho, B. Cunha, A.S. Moreira, A. Xenopoulos, P.M. Alves, M.J.T. Carrondo, C. Peixoto, Membrane-based approach for the downstream processing of influenza virus-like particles, Biotechnol. J. 14 (2019) 1800570, https://doi.org/10.1002/biot.201800570.

[8] S.R. Wickramasinghe, B. Kalbfuß, A. Zimmermann, V. Thom, U. Reichl, Tangential flow microfiltration and ultrafiltration for human influenza A virus concentration and purification, Biotechnol. Bioeng. 92 (2005) 199–208, https://doi.org/10.1002/bit.20599.

[9] B. Wu, F. Xiao, P. Li, Y. Du, J. Lin, K. Ming, B. Chen, X. Lei, B. Xu, D. Liu, Ultrasensitive detection of serum hepatitis B virus by coupling ultrafiltration DNA extraction with real-time PCR, PloS One 12 (2017), e0170290, https://doi.org/10.1371/journal.pone.0170290.

[10] A. Negrete, A. Pai, J. Shiloach, Use of hollow fiber tangential flow filtration for the recovery and concentration of HIV virus-like particles produced in insect cells, J. Virol. Methods 195 (2014) 240–246, https://doi.org/10.1016/j.jviromet.2013.10.017.

[11] E.E. Borujeni, Y. Li, A.L. Zydney, Application of periodic backpulsing to reduce membrane fouling during ultrafiltration of plasmid DNA, J. Membr. Sci. 473 (2015) 102 108, https://doi.org/10.1016/j.memsci.2014.08.059.
[12] F. Meacle, A. Aunins, R. Thornton, A. Lee, Optimization of the membrane purification of a polysaccharide-protein conjugate vaccine using backpulsing, J. Membr. Sci. 161 (1999) 171 184, https://doi.org/10.1016/S0376-7388(99)00111-8.
[13] G. Tkacik, S. Michaels, A rejection profile test for ultrafiltration membranes & devices, Bio Technol. 9 (1991) 941 946, https://doi.org/10.1038/nbt1091-941.
[14] S. Mochizuki, A.L. Zydney, Dextran transport through asymmetric ultrafiltration membranes: comparison with hydrodynamic models, J. Membr. Sci. 68 (1992) 21 41, https://doi.org/10.1016/0376-7388(92)80147-C.
[15] J.I. Calvo, R.I. Peinador, V. Thom, T. Schleuss, K. ToVinh, P. Pradanos, A. Hernandez, Comparison of pore size distributions from dextran retention tests and liquid-liquid displacement porosimetry, Microporous Mesoporous Mater. 250 (2017) 170 176, https://doi.org/10.1016/j.micromeso.2017.05.032.
[16] S.R. Wickramasinghe, S.E. Bower, Z. Chen, A. Mukherjee, S.M. Husson, Relating the pore size distribution of ultrafiltration membranes to dextran rejection, J. Membr. Sci. 340 (2009) 1 8, https://doi.org/10.1016/j.memsci.2009.04.056.
[17] M. Bakhshayeshi, H. Zhou, C. Olsen, W. Yuan, A.L. Zydney, Understanding dextran retention data for hollow fiber ultrafiltration membranes, J. Membr. Sci. 385 386 (2011) 243 250, https://doi.org/10.1016/j.memsci.2011.09.047.
[18] M. Bakhshayeshi, A. Teella, H. Zhou, C. Olsen, W. Yuan, A.L. Zydney, Development of an optimized dextran retention test for large pore size hollow fiber ultrafiltration membranes, J. Membr. Sci. 421 422 (2012) 32 38, https://doi.org/10.1016/j.memsci.2012.06.020.
[19] V. Tirtaatmadja, D.E. Dunstan, D.V. Boger, Rheology of dextran solutions, J. Non-Newtonian Fluid Mech. 97 (2001) 295 301, https://doi.org/10.1016/S0377-0257(00)00226-3.
[20] L.J. Zeman, A.L. Zydney, Microfiltration and Ultrafiltration: Principles and Applications, Marcel Dekker, 1996.
[21] J.C. Giddings, E. Kucera, C.P. Russell, M.N. Myers, Statistical theory for the equilibrium distribution of rigid molecules in inert porous networks, J. Phys. Chem. 72 (1968) 4397 4408, https://doi.org/10.1021/j100859a008.
[22] K.A. Granath, Solution properties of branched dextrans, J. Colloid Sci. 13 (1958) 308 328, https://doi.org/10.1016/0095-8522(58)90041-2.
[23] D.R. Latulippe, J.R. Molek, A.L. Zydney, Importance of biopolymer molecular flexibility in ultrafiltration processes, Ind. Eng. Chem. Res. 48 (5) (2008) 2395 2403, https://doi.org/10.1021/ie8005337.